Advanced Engineering Materials

ADVANCED ENGINEERING MATERIALS
www.aem-journal.com

RESEARCH ARTICLE OPEN ACCESS

On the Influence of Antioxidants and Recycled MgO–C Source Material on the Mechanical Properties of Carbon-Bonded Magnesia Refractories

Marc Neumann[1] | Tom Weber[1] | Jana Hubálková[1] | Florian Kerber[1] | Dinesh Kumar Gunasekar[1] | Hans Jelitto[2] | Christos G. Aneziris[1]

[1]Institute of Ceramics, Refractories and Composite Materials, Technical University Bergakademie Freiberg, Freiberg, Germany | [2]Institute of Advanced Ceramics, Hamburg University of Technology, Hamburg, Germany

Correspondence: Marc Neumann (marc.neumann@ikfvw.tu-freiberg.de)

Received: 15 October 2025 | **Revised:** 15 January 2026 | **Accepted:** 5 February 2026

Keywords: antioxidants | carbon-bonded magnesia | R-curve behaviour | recyclates | refractoriness under load | Youngs' modulus

ABSTRACT

In the present study, the role of recycled source material and the addition of antioxidants to refractory MgO–C material commonly used in the steel industry were addressed from the perspective of fracture mechanics. Initially, the fracture behaviour of the fine grained MgO–C-matrix was assessed by sequential bending experiments (particle sizes <150 µm). Based on this, coarse grained parts with particle sizes up to 7 mm were prepared and characterised in regard to their high-temperature properties, i.e. the refractoriness under load, the thermal expansion behaviour and the Young's modulus as function of the temperature. Four differently designed batches were tested. One batch, consisting of all fresh source materials (MgO and C), served as reference. Furthermore, the additives Al, SiO_2 and TiO_2 were systematically added, and 50% of the source material was replaced by recycled MgO–C from the industry. During the batch production, environmentally friendly fructose, collagen and lignin served as temporary binding agents. It was found that while the addition of recycled MgO–C had a reducing effect on the mechanical properties, the opposite was observed for the addition of antioxidants.

1 | Introduction

Since the development of steelmaking, there has been a steady increase in the demand for steel. In 1950, the worldwide steel production totalled 207 million tons [1]. Within 74 years that number increased up to 1885 million tons in 2024 [2]. Combined with the fact that steelmaking is a high-temperature process, the need for refractory materials is inevitable. During steelmaking, the refractory materials are under heavy load due to corrosion and thermal stresses, causing them to wear out. From 1970 to 2010, the refractory consumption fell from 25 to 30 kg per ton of steel to 8 kg per ton of steel. Up to 40 million tons of refractories are produced each year, 70% of which is used by the steel industry. Due to the favourable prices of the source materials and low disposal costs for worn out refractories, the recycling never received much attention [3, 4]. Nevertheless, the recycling of used refractories plays an increasing role because of the environmental concerns, the amount of emitted CO_2 during production and the dependence of volatile market participants. Carbon-bonded (MgO–C) refractories are widespread materials due to their advantageous properties regarding thermal and chemical behaviour. These properties are still present after their primary application even if there are certain compromises in terms of porosity and impurities [5]. Nevertheless, the renewed use of recycled materials is a promising approach and in order to successfully replace virgin source materials with recycled materials it is essential to investigate their mechanical properties. These findings are crucial to understand the behaviour and justify their usage in future applications. With the combination of recycled MgO–C material from previous applications and environmentally

friendly binders, the refractory industry can take a major step towards a more sustainable, closed-loop circular economy.

Common practice in the fabrication of MgO–C refractories is the application of phenol formaldehyde-based resins as binding agents. Even though they provide the desired characteristics of a binder, e.g. long-term stability, they are noxious for the environment and carcinogenic [6, 7]. Therefore, the need for environmentally friendly binders based on new approaches is desirable. Such environmentally friendly binders are typically based on hydrocarbons such as sucrose, fructose or lactose. Other binding agents could be lignin and collagen [4, 8]. During thermal processing, lignin undergoes cross-linking comparable to that of tar- and pitch-based resins. Collagen exhibits a similar behaviour while maintaining its desired mechanical properties even at elevated temperatures.

Regarding the application at elevated temperatures, carbon-bonded materials such as MgO–C may face a troublesome decarburisation during high-temperature process, which impairs their performance tremendously. A way to hinder decarburisation is the addition of metal-based powders like Al or low-melting oxides such as TiO_2 [9, 10]. It was shown that the addition of Al prevents the oxidation of the carbon, as Al_4C_3 is formed instead as a reaction product with the graphite contained in the MgO–C. This can be partially oxidised by CO to form Al_2O_3 or react with existing N_2 to form AlN whiskers, which also reinforce the microstructure [9]. Comparable results were found for the addition of TiO_2, namely the formation of TiCN or TiN [10]. Apart from this, the addition of SiO_2 was found to further improve the properties of the refractory material [7].

Among other features, the fracture behaviour and the high-temperature properties thus pose design-relevant properties in order to guarantee orderly function and service life. Therefore, the addition of recycled source materials and the application of environmentally friendly binding agents have to be benchmarked from the mechanical point of view. Besides, the addition of antioxidants is a promising approach, yet to be evaluated in terms of the fracture resistance. Reviewing the literature, the properties of MgO–C and the potential of the above-mentioned approaches were already addressed by several authors [10–18]. To a certain extend, the influences of recycled source material, environmentally friendly binding agents or antioxidants on the mechanical properties of MgO–C such as the strength or Young's modulus were indeed covered by those studies before. However, the literature falls short regarding other fracture mechanical data, for example the critical stress intensity as a measure of the fracture resistance and especially for fine-grained carbon-bonded magnesia. Against this background, the characterisation within this paper was divided. First, the influence of the addition of antioxidants and the replacement of half of the source material with recycled MgO–C on the fracture resistance of the fine-grained 'matrix' (particle sizes <150 μm) was investigated. Derived from previous studies, the partial substitution of the source material with up to 50% recycled MgO–C, a decrease in the fracture resistance may be presumed [7]. The general scale of the fracture resistance and to which extend the addition of antioxidants may counteract the effect of the recycled source material are the central research questions of this first part. Based on this, in a second step, coarse grained bulk parts with particle sizes up to 7 mm were tested with regard to refractoriness under load (RuL), thermal expansion (TE) behaviour and Young's modulus at elevated temperatures. Tying into the research questions of the first part, the influence of the fracture behaviour of the fine matrix on the resulting properties of the coarse-grained bulk parts shall be discussed.

2 | Experimental Section

2.1 | Sample Preparation

All samples were produced via uniaxial pressing on a hydraulic press ES270 (RUCKS Maschinenbau GmbH, Germany). The premixing of the batches with the compositions as listed in Table 1 was performed in a conventional mortar mixer ToniMIX (ToniTechnik Baustoffprüfsysteme GmbH, Germany) [19].

For the fine-grained matrix batches M to M-AR, the available fractions FM 0–1 mm, R-FM 0–1 mm and DBM were sieved and only the grains finer than 150 μm were used in the preparation.[1] The maximum pressure during the uniaxial pressing amounted to 120 MPa for the batches M to M-AR and 150 MPa for the batches C to C-AR. Both the M- and C-batches were pressed into rectangular samples of approximately $6.5 \times 9.5 \times 70\ mm^3$ (M) and $25 \times 25 \times 150\ mm^3$ (C). Beyond that, cylinders of 50 × 50 mm (height × diameter) were prepared from the C-batches by uniaxial pressing at 150 MPa as well.

After pressing, the samples were dried and cured according to the following procedure: In the first step, the samples were heated to 85°C with a heating rate of 600 K h^{-1} and a dwell time of 2 h. In a second step, they were further heated to 220°C with a heating rate of 55 K h^{-1} and a dwell time of 1 h. This was followed by a free cooling within the furnace. Finally, the samples were coked at 1000°C with a heating rate of 100 K h^{-1} and a dwell time of 3 h, again followed by free cooling within the furnace. The coking was realised by embedding the samples in pet coke. After coking, all samples were stored in a desiccator until testing to prevent moisture absorption.

2.2 | Characterisation

2.2.1 | Fine-Grained Matrix

The samples of the fine-grained batches M to M-AR were intended for sequential four-point bending experiments at the Institute of Advanced Ceramics at the Hamburg University of Technology to evaluate the fracture resistance and a potential R-curve behaviour. A profound insight, i.e. the specific experimental procedure, the used equipment and the principles of the data analysis, is outlined elsewhere [20–22]. The main objective of the sequential testing is to initiate and control stable crack growth. After each loading sequence, the load is released partially so that crack growth would be arrested. In the presented study, the loading was realised deflection controlled with a rate of 0.02 μm s^{-1}, while the partial releases were performed with a rate of 10 μm s^{-1}. The standard number of loading sequences amounted to about 10–25, after which the sequential testing was terminated, i.e. generally when the sample was still intact and not fully broken. It was possible to initiate and control a stably growing crack in samples of all test series M to M-AR. The crack path was investigated after the sequential testing by the aid of μCT using a micro focus X-ray computed tomograph CT-Alpha

TABLE 1 | Batch composition (M-fine-grained matrix batches, C-coarse-grained batches, A addition of antioxidants, R use of recycled source material, AR addition of antioxidants and use of recycled source material; all in mass%; amounts of aluminium, silica, and titania relative to the solid mass; all suppliers from Germany).

	Suppliers	M	M-A	M-R	M-AR	C	C-A	C-R	C-AR
FM, 3–7 mm	Refratechnik Steel GmbH	—	—	—	—	21.14	21.14	10.57	10.57
FM, 1–3 mm		—	—	—	—	34.01	34.01	17.11	17.11
FM, 0–1 mm		—	—	—	—	22.98	22.98	11.49	11.49
FM, 0–1 mm (<150 μm)		78.14	78.14	39.07	39.07	—	—	—	—
R-FM, 3–6 mm	Refratechnik Steel GmbH	—	—	—	—	—	—	10.57	10.57
R-FM, 1–3 mm		—	—	—	—	—	—	17.11	17.11
R-FM, 0–1 mm		—	—	—	—	—	—	11.49	11.49
R-FM, 0–1 mm (<150 μm)		—	—	39.07	39.07	—	—	—	—
DBM	Refratechnik Steel GmbH	—	—	—	—	13.79	13.79	13.79	13.79
DBM (<150 μm)		13.79	13.79	13.79	13.79	—	—	—	—
Graphite (NFL)	Graphit Kropfmühl AG	3.06	3.06	3.06	3.06	3.06	3.06	3.06	3.06
Carbon Black (CB)	Lehmann & Voss & Co.	0.92	0.92	0.92	0.92	0.92	0.92	0.92	0.92
Fructose	Gellmi, Hanseatische Zuckerraffinerie	3.17	3.17	3.17	3.17	2.45	2.45	2.45	2.45
Lignin	TCI Deutschland GmbH	0.31	0.31	0.31	0.31	0.31	0.31	0.31	0.31
Collagen	FNW International GmbH	0.61	0.61	0.61	0.61	0.61	0.61	0.61	0.61
Aluminium (Al)	Carl Roth GmbH & Co. KG	—	2.50	—	2.50	—	2.50	—	2.50
Silica (SiO_2)	RW silicium GmbH	—	0.50	—	0.50	—	0.50	—	0.50
Titania (TiO_2)	Crenox GmbH	—	0.40	—	0.40	—	0.40	—	0.40

(Procon X-ray GmbH, Germany), equipped with a Dexela detector (1944 × 1526 pixel, type 1512, Perkin Elmer Inc., Canada).

For the sequential bending tests, a notch had to be machined into the samples. The notch was in line with the direction of pressing, i.e. alongside the sample height of 9.5 mm. The majority of the notch, approximately 2.2 mm, was cut by a diamond saw blade. The remaining approximately 0.8 mm were inserted by razor blades covered with diamond pastes of a mean particle size of 15 μm and 1 μm. The notch preparation was done in the cured state, i.e. before coking, in order to heal unwanted damage ahead of the notch tip. The final macroscopic notch depth after coking was determined optically on the sample surface. The general relative macroscopic notch depth amounted to 32%. For the determination of the R-curve, the room temperature Young's modulus E_0 after the coking and the Poisson ratio ν were required. The latter was assumed with $\nu = 0.35$, representing rather porous materials. The Young's modulus of each batch after coking was estimated on the basis of 17 coked and un-notched beam samples using the impulse excitation technique, i.e. following the principles of the DIN EN 843-2:2007 standard.[2] Each sample was excited manually, and the vibration of the sample was recorded acoustically via microphone. The signal was then transformed into a frequency spectrum via Fourier-transformation, and the natural flexural frequency f_0 was derived. The room temperature Young's modulus E_0 then followed Equation (1):

$$E_0 = 0.946\left(\frac{m f_0^2 l^3}{b w^3}\right)\left(1 + 6.585\left(\frac{w}{l}\right)^2\right) \quad (1)$$

where m is the sample mass, w is the sample thickness, b is the sample width and l is the sample length. Besides, the geometric density and the volume change after the coking were recorded based on the sample dimensions and the sample mass. Due to their rectangular and overall regular shape, the geometric density equals the bulk density of the samples. In addition to that, hydrostatic weighing was performed in toluene for coked spare samples allowing for a comparison of the M-batches in terms of the open porosity (three samples were tested per batch). The microstructure was investigated at polished fracture surfaces of manually broken coked spare samples via scanning electron microscopy (SEM) using an XL30 ESEM FEG D1511 (FEI, Netherlands).

2.2.2 | Coarse-Grained Parts

The characterisation of the coarse grained batches C to C-AR comprehended the evaluation of the thermal expansion (TE) and the refractoriness under load (RuL). Both were determined on the cylindrical samples in a RUL/CIC 421 Bell furnace (NETZSCH, Germany). The maximum testing temperature was set to 1600°C with a heating rate of 5 K min^{-1}. The load during the RuL measurements (cf. DIN EN ISO 1893) was 0.2 MPa, while only a minimum load of 0.01 MPa was applied during the TE tests to ensure contact to the position encoder. For either of these high-temperature tests, the furnace was purged with argon to prevent the samples from oxidation. To further protect the cylinders from loss of carbon, the mantle surface of the cylinders was coated with a carbon black (CB) paste acting as a sacrificial protection layer.

Additionally, the Young's modulus E_T was determined as function of the temperature, again employing the impulse excitation technique. The measurements followed the principles of the ASTM E1876 standard and were performed in a RFDA HTVP1600 device (IMCE, Belgium) under an argon atmosphere. The heating rate amounted to 5 K $min^{-1,}$ and a dwell of 20 min was set at the maximum testing

temperature of 1350°C. Afterwards, the cooling was realised with a rate of 3 K min^{-1}. During the measurement, the sample was excited with a corundum projectile every 60 s and again the vibration of the sample was recorded via microphone and converted into the natural flexural frequency f_T at the respective temperature. Before testing at elevated temperatures, the Young's modulus was determined at room temperature, as previously described for the fine-grained materials. The Young's modulus E_T at an elevated temperature T was then calculated according to Equation (2):

$$E_T = E_0 \left(\frac{f_T}{f_0}\right)^2 \left(\frac{1}{1+\alpha\Delta T}\right) \quad (2)$$

with E_0 and f_0 again being the room-temperature Young's modulus and the flexural frequency, and α being the coefficient of thermal expansion.

Based on the characterisation of fine-grained batches, the geometric density after coking and the volume change of the coarse-grained batches were determined in equal measure. Since they served for comparative purposes only, the geometric density after coking and the coking shrinkage were determined for only five randomly selected coarse-grained beams. In line with the characterisation of the M-batches, hydrostatic weighing was also performed for three coked coarse-grained spare beams of the C-batches. The immersion liquid was again toluene. The data processing of all of the subsequently presented results was done in the free software package 'R' [23].

3 | Results and Discussion

3.1 | Microstructure and Basic Physical Properties

Figure 1 shows SEM micrographs of polished fracture surfaces of the M-batches. The basic microstructural units are the MgO-grains, the carbon matrix and voids such as pores, delamination gaps between the matrix and the MgO-grains and microcracks within the MgO-grains. Apart from those units, grains that are silicon- and calcium-enriched were found in the M batch, indicating that those originate from the fresh MgO source material (bright spot x_1 in Figure 1a). For the M-A and M-AR batch, grains were observed that are enriched with calcium, silicon and titanium. In M-AR, there were also traces of aluminium (cf. x_4 Figure 1d). Besides, pure aluminium particles were found in those two batches as well. All those observations are in good agreement to the batch composition listed in Table 1. Owing to the grain sizes up to 7 mm and the theoretically required very low magnification, SEM micrographs of the C-batches are omitted. Nonetheless, the micropraghs of the M-batch structures also represent the fine matrix present in the C-batches. As those micrographs only serve as an overview, the structural evaluation shall not be further deepened at this point. A more in-depth insight into the structure of MgO–C and the influence of antioxidants and recycled source materials are presented elsewhere [5, 10].

The basic physical properties of the investigated materials comprise permanent volume change during the coking ΔV_{coking}, the bulk density ρ_{bulk} after coking and the room-temperature Young's modulus E_0 after coking, see Figure 2. For comparison reasons, the data of the M- and C-batches are plotted next to each other. As presented, the permanent volume change of the M batch was negative indicating shrinkage, at maximum −1%. The addition of antioxidants reversed the sign of the permanent volume change meaning volumetric expansion, as shown for M-A. Besides, the scattering among the different samples of M-A was increased (wider box), even outliers were observed. The scatter may be reduced by paying proper attention during the homogenisation, which is certainly achievable on an industrial scale. A similar effect of the antioxidants was observed for the batches M-R and M-AR. The major part of the box of M-R was below zero, hence the samples shrunk. In turn, the M-AR

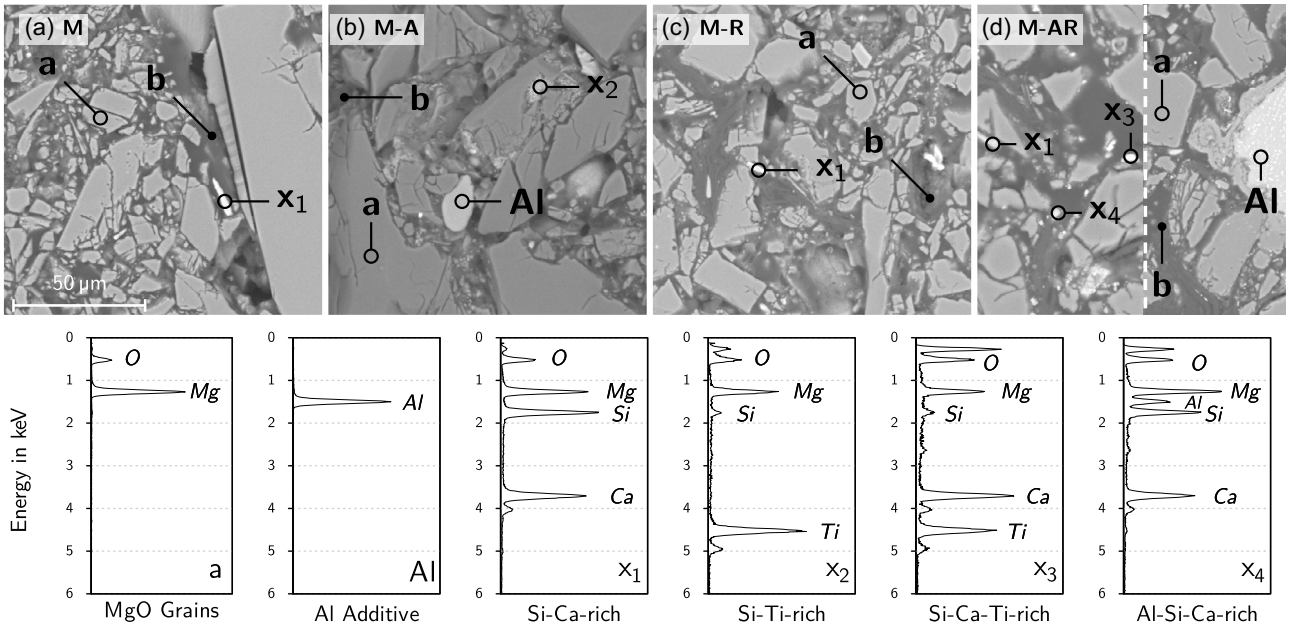

FIGURE 1 | SEM micrographs of polished fracture surfaces of the M-batches and EDX scans (spot analysis at the centre of the open circles) of the microstructural units (BSE-mode; a-MgO grains, b-carbon matrix, Al-aluminium particles, x_1-Si–Ca-enriched, x_2-Si–Ti-enriched, x_3-Si–Ca–Ti-enriched, x_4-Al–Si–Ca-enriched, black-pores and micro cracks; any other bright spots fall under one of the listed categories). SEM = scanning electron microscopy.

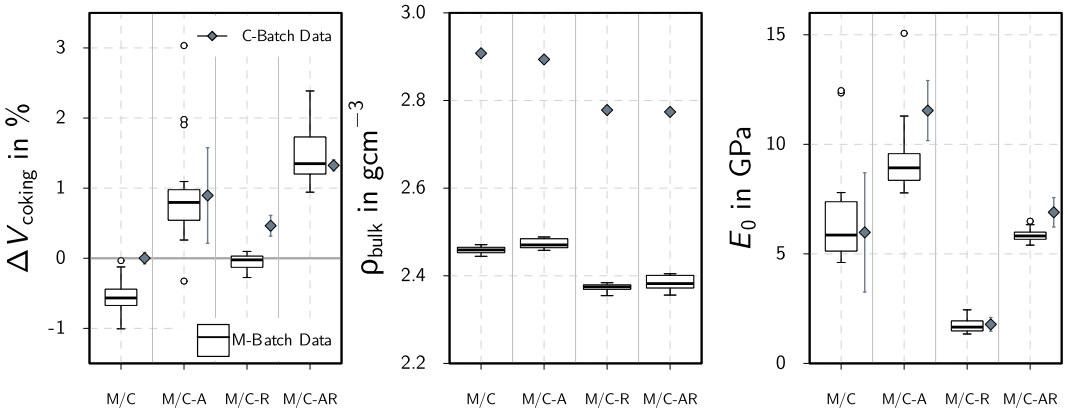

FIGURE 2 | Overview on the basic physical properties of the fine-grained M-batches and the coarse-grained C-batches, i.e. the permanent volumetric change ΔV_{coking}, the bulk density ρ_{bulk} and the Young's modulus E_0, each after coking (the boxplots of the M-batch data were developed from 17 individual samples, circles indicate outliers; grey diamonds and error bars indicate averaged data from the coarse-grained C-batches including the standard deviation, based on five C-batch beams.).

samples expanded during the coking, also yielding the highest absolute permanent volume changes of all series. Again, the addition of the antioxidants increased the scattering among the samples (wider box and wider whisker spans). Regardless of whether antioxidants were added or not, the partial replacement of MgO by recycled MgO–C resulted in an overall shift of the permanent volume change towards positive values, i.e. volumetric expansion. The overall effect was also observed for the coarse-grained C-batches. In particular, the permanent volume change of the all fresh reference batch C was close to zero, while the permanent volume change of C-A, -R and -AR were positive. These effects should be kept in mind during the manufacturing process in order to meet the required net shape dimensions after the coking. Turning to the resulting bulk density, the addition of antioxidants had a minimal effect, while the use of recycled source material caused lower densities. This may trace back to a lower true density of the recycled source material.

The bulk density of all of the coarse-grained C-batches were higher than those of the fine-grained M-batches. This is largely attributed to the particle packing density in particular. The particle packing was intentionally designed for the C-batches, while the M-batches were developed by removing the coarse fractions without re-adjusting the particle size distribution model. The intention of which was to isolate the properties of the matrix as it would be present in the coarse-grained parts without influencing the ratio of the fine-grained fractions to each other. Table 2 lists the results of the hydrostatic weighing interpreted in terms of the open porosity π_o and the bulk density $\rho_{b.hw}$. The latter match the scales of the resulting geometric bulk densities from Figure 2, further verifying the above-discussed aspects. In line with that, the open porosity of the M-batches is higher than those of the C-batches by a factor of three. Among the M-batches, the open porosity is about equal. Consequently, the differences in the bulk density in the M-batches trace back to a variant closed porosity. The open porosities of the C-R- and C-AR-batch, both containing recycled source material, were higher by approximately 1% to 2% higher when compared to C or C-A, which basically complies with the resulting bulk densities of the C-batches. That probably traces back to volatiles contained in the recycled source materials, whose escape during coking cannot be prevented completely (for instance residual pitch, resin, etc.) [4].

The Young's modulus after coking was affected by the addition of antioxidants similarly to the permanent volume change. When again grouping according to the used source materials and comparing the data within the respective group, the Young's modulus was higher after the addition of Al, TiO_2 and SiO_2. Apart from that, the partial replacement of the source materials with recycled MgO–C had a striking impact as well. By comparing either M and M-R or C and C-R, the Young's modulus was reduced by a factor of 3–4. That decrease was counteracted by the addition of antioxidants though, i.e. the mean level of the Young's modulus was about the same for M and M-AR or C and C-AR, respectively. However, the highest Young's modulus was observed for M-A and C-A, i.e. for all-fresh source materials in combination with antioxidants. Hence, the Young's modulus was different regardless that the bulk densities of M and M-A or C and C-A were basically similar. Like presented before, the open porosity of the M-batches was about similar and the open porosities of the C-batches differed only to a small amount.

TABLE 2 | Open Porosity π_o and bulk density $\rho_{b.hw}$ of the M- and C-batches (both obtained from hydorstatic weighing in toluene).

	M	M-A	M-R	M-AR
π_o in Vol%	27.30 ± 0.50	28.20 ± 2.00	28.90 ± 2.10	28.40 ± 2.70
$\rho_{b.hw}$ in gcm^{-3}	2.53 ± 0.01	2.48 ± 0.07	2.37 ± 0.08	2.39 ± 0.10
	C	**C-A**	**C-R**	**C-AR**
π_o in Vol%	9.88 ± 0.66	9.85 ± 0.11	11.15 ± 0.33	10.75 ± 0.11
$\rho_{b.hw}$ in gcm^{-3}	3.01 ± 0.01	2.96 ± 0.04	2.88 ± 0.01	2.86 ± 0.01

Consequentially and as discussed for the bulk densities, the differences in the Young's modulus hint for differences in the closed porosity. Derived from Figure 2, the addition of antioxidants would then result in less closed porosity as M/C-A and M/C-AR have higher Young's moduli than M/C and M/C-R, respectively. The extent to which this conclusion is justified requires further investigation, taking into account other microstructural effects of adding antioxidants. Therefore, the above statement is a theoretical one that could be investigated in future studies.

In sum, it was found that the addition of antioxidants affects the resulting mechanical properties even at room temperature, as was shown for the Young's modulus, for example. This effect was already observed by Luz et al. [24]. Khezrabadi et al. [25] also found that the addition of Al to carbon-bonded ceramics also has a strength-enhancing effect. In order to test this hypothesis for the present MgO–C materials, the following section will provide an insight into the fracture behaviour, namely the R-curve as a measure of fracture resistance.

3.2 | R-Curve Behaviour

The R-curves, meaning the fracture resistance K_{IR} as a function of the crack extension Δa, obtained from the sequential bending experiments are plotted in Figure 3a. Apparently, an R-curve behaviour was observed for all materials, albeit to varying degrees in terms of steepness and the difference between the initial and plateau values. The experimental data could be modelled successfully according to the following Equation (3) (the model parameters are listed in Table 3) [26]. The model curve of M revealed that M may have certain potential for further increase in K_{IR} beyond crack extensions Δa of 3500 µm. Nonetheless, the main toughening was observed within the presented range Δa. Strictly focusing on the raw data points (black circles), a plateau could be assumed for M for $\Delta a \geq 2500$ µm. Since the R-curve modelling of the M data resulted in a coefficient of determination $R^2 > 0.98$, the determined model is still considered as a suitable measure and properly reflects the given data. The same applies to the batches M-A and M-AR. For M-R, a clear plateau was found above 500 µm, both in the raw data (red circles) and in the model (red solid line).

TABLE 3 | Fitting parameters according to Equation (3).

ID	K_{I0}^{mod} in MPa$\sqrt{m}$	p in MPa$\sqrt{m}$	q in 1/$\sqrt{\mu m}$
M	0.0238	0.3962	0.0211
M-A	0.0337	0.2406	0.0647
M-R	0.0200	0.0321	0.1023
M-AR	0.0333	0.3443	0.0303

The trend established for the room-temperature Young's modulus was confirmed in the R-curve data as well. Taking M as reference (all fresh source materials without antioxidants; solid black line in subfigure (a) of Figure 3), the following was found: The addition of antioxidants has an enhancing effect (M-A) while the partial replacement of the source materials by recycled MgO–C has a reducing effect (M-R), which is counteracted by the antioxidants (M-AR) even exceeding the reference level. The total range of the K_{IR}-values was in the range of KPa$\sqrt{m}$, which is low when compared to common K_{IR} data from technical ceramics like Al_2O_3 or Si_3N_4, or other refractory materials like MgO [26–29]. The low K_{IR}-values are a consequence of the carbon bonding, i.e. the packing of the ceramic MgO grains inside a carbon matrix rather than sintering the MgO grains together. To separate these carbon–magnesia interfaces, which form almost no chemical bond, less energy is required than for the creation of new surface by separating two sintered MgO grains, hence leading to the overall lower fracture resistance. In fact, a lowered fracture toughness was observed for carbon-bonded Al_2O_3–C and carbon-bonded MgO–C [13, 30–33]. However, especially the K_{IR}-values for MgO–C were determined for coarse-grained parts with maximum grain sizes above 1 mm. In such coarse-grained materials, both crack bridging (due to the large grains spanning the crack) and crack branching (along the enlarged matrix-grain interfaces along the large grains) can become more pronounced, resulting in higher fracture resitances than those observed in the

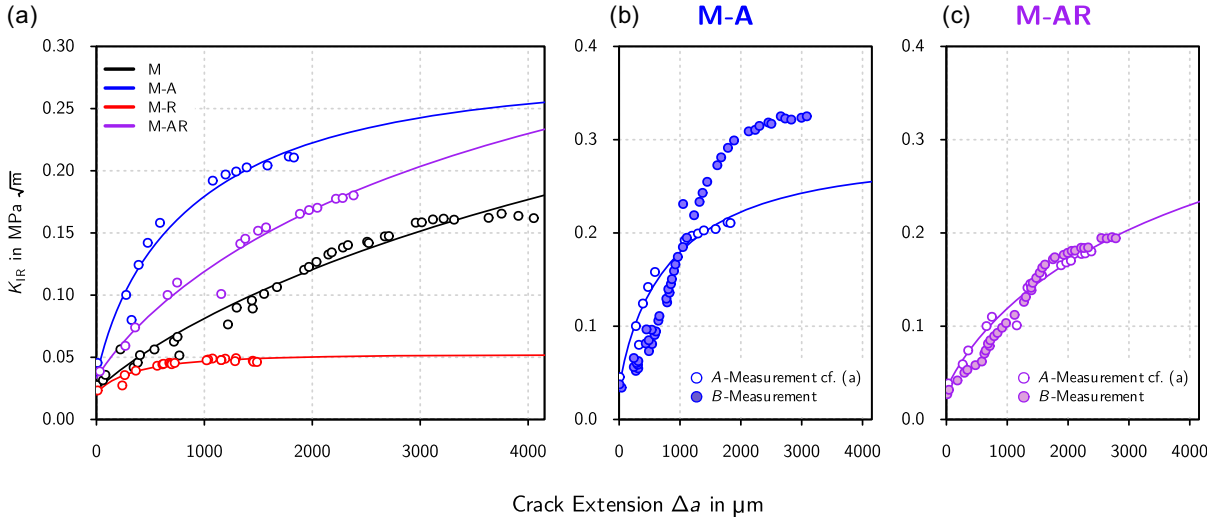

FIGURE 3 | R-curve behaviour of the fine-grained M-batches: (a) *A*-measurements with standard number of loading sequences <30 of all four M-batches and (b,c) *B*-measurements with higher number of loading sequences >30 of the M-A and M-AR batch (solid lines: fitted literature model according to Fünfschilling et al. [26]).

present study. The results obtained by Hino et al. [13, 31] and Solarek et al. [33], in conjunction with the results of this study, thus highlight the potential inherent in the use of coarse-grained components, which can be further exploited by making adjustments to the fine matrix. Besides and derived from Figure 2, M-batch materials showed a certain porosity further lowering the fracture resistance [34, 35].

$$K_{IR} = K_{I0}^{mod} + p\left[1 - (1 + q\sqrt{\Delta a})\exp(-q\sqrt{\Delta a})\right] \quad (3)$$

The potential toughening mechanisms that act in favour of the fracture resistance and cause the R-curve behaviour of the MgO–C materials are assumed to be found among crack deflection and crack branching [36]. Due to crack deflection, the crack path deviates from a straight line and thus a larger crack surface has to be created in order to fully separate the body into parts requiring more energy to be applied. A pronounced three-dimensional crack deflection could indeed be visualised for the M-batches via μCT. It is exemplarily presented in Figure 4 for M-AR. For crack branching, secondary cracks form/branch from the major primary crack at the tips of which energy is also dissipated. This energy is then lacking for the crack advance of the primary crack. These two mechanisms occur preferentially along the inner phase boundaries, i.e., favoured by the MgO–C microstructure with its ceramic-carbon interfaces. Besides, the crack deflection leaves roughed up crack surfaces in the crack wake, i.e. behind the crack tip. Across those roughed up surfaces, a certain level of stress can be transferred via friction when in contact to each other, i.e. the crack is bridged. This crack bridging shields the crack tip, i.e. it reduces the effectively applied stress intensity at the tip of the crack. This further promotes the R-curve behaviour. It should be noted that sequential testing might degrade such toughening mechanisms [29, 37]. Effectively, that would result in an underestimation of the R-curve. Since this is a conservative approach, it is assumed to be reasonable.

For the batches M-A and M-AR, i.e. the most promising batches due to their level of K_{IR}, additional sequential measurements were performed in order to gain information about the R-curve data variation (*B*-measurements). A difference in the data variation was already noted for the Young's modulus data, where M-A showed higher variation than M-AR. During the *B*-measurements, the number of load sequences was increased resulting in a higher resolution along the R-curve. The results are presented in Figure 3b,c. Whilst the magnitude and character of the R-curve data was again verified, the deviation among the individual measurements was more pronounced for M-A than for M-AR. This is hence consistent with the Young's modulus data presented in Figure 2. This emphasises the role of the antioxidants and the potential role of the packing/densification during the pressing, both factors which may increase the Young's modulus and thus help to exploit the R-curve potential to its maximum. Besides, these observations support the findings of Khezrabadi et al. [25] mentioned before.

A closing note on the *B*-type R-curves shall be given regarding the modelling according to Fünfschilling et al. [26]. As presented in Figure 5, the fitting of the M-A and M-AR *B*-measurement R-curve data according to Equation (3) would be successful. Despite coefficients of determination of $R^2 > 0.96$, the R-curve plateaus are falsely estimated. In the case of M-A, also the initial stage of the R-curve is represented non-accurately.[3] The modelling would predict a further increase in K_{IR}, which contradicts the raw data that provide strong evidence of the onset of a

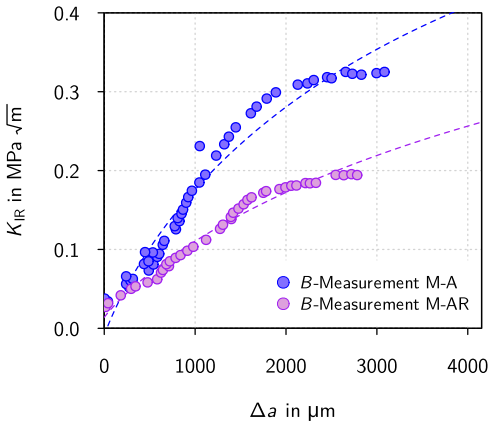

FIGURE 5 | R-curve modelling of the *B*-measurements of M-A and M-AR batches (dashed lines: fitted based on Equation (3)).

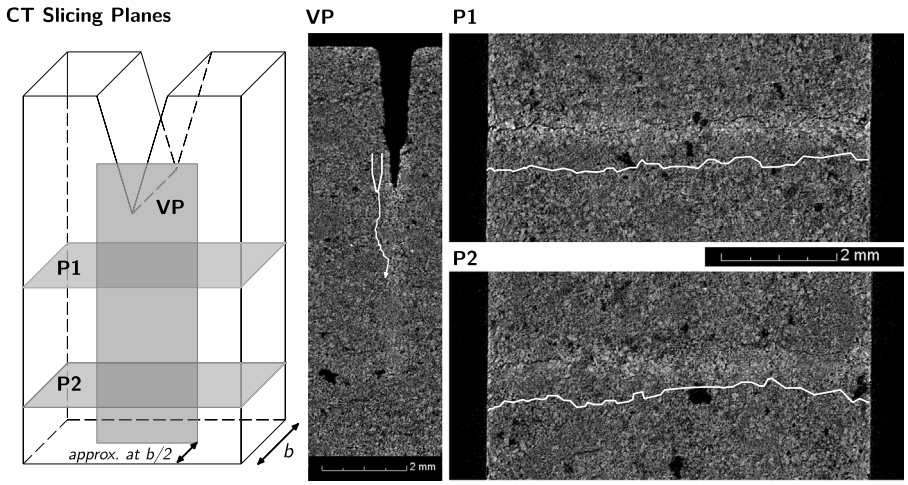

FIGURE 4 | Crack monitoring via micro focus X-ray computed tomography CT, exemplarily shown for M-AR (left: concept of slicing with *b* being the sample width; right: reconstructed CT images, crack path retraced in white).

plateau. Probably, modelling the first stage of the R-curve data of the *B*-measurements in the range of $\Delta a = 1000\,\mathrm{MPa}\sqrt{\mathrm{m}}$, which appeared exponential for M-A and quasi-linear for M-AR, and simultaneously accounting for the plateau at $\Delta a > 1500\,\mu\mathrm{m}$ demands adjustments in the mathematical model. This, however, poses an issue to be addressed in the future and as a consequence, the modelling of the *B*-measurements was waived in the present paper, since a broader data basis is required.

The mechanical properties of the matrix material at room temperature present the baseline for the performance of the coarse-grained MgO–C materials at elevated temperatures. For instance, the higher the crack resistance and the more pronounced an R-curve is, the higher is the thermal shock damage tolerance. Consequently, the batches M-A and M-AR are the most promising for an application at elevated temperatures. These findings shall be validated for the coarse-grained C-batches in the subsequent section.

3.3 | High-Temperature Properties

The high-temperature properties were examined for the coarse-grained C-batches only, since they are close to the composition of industrial bricks. The thermal expansion TE and the refractoriness under load RuL of the C-batches are presented in Figure 6. The addition of antioxidants (C vs. C-A) as well as partially using recycled source materials (C and C-A vs. C-R and C-AR) both result in lower coefficients of thermal expansion α. The impact of using recycled material is more pronounced than the impact of adding antioxidants. The interaction of both was neglectable as the difference between C-R and C-AR only occurs in the second decimal digits.

The RuL results are in sound agreement with the TE data. The application of recycled material caused the RuL curves to drop at lower temperatures compared to the batches with merely fresh source materials (C and C-A vs. C-R and C-AR). The refractoriness is thus lowered. In turn, the simultaneous addition of antioxidants improves the RuL of the C-batches with recycled source material (cf. C-R vs. C-AR), where the $T(\mathrm{d}L\,\mathrm{max})$ is raised by more than 40°C. The same conclusion could be drawn from the comparison of the batches C and C-A, yet the improvement was less pronounced. Besides, for the batches C-R and C-AR the overall extension during the RuL tests was lower by more than 0.5%. Summarising these results, the addition of antioxidants Al, SiO_2 and TiO_2 render a promising tool to adjust the high-temperature performance under high-temperature load as well as reducing the thermal expansion (if desired). Fine adjustments based on composition of C-AR regarding the added antioxidants may also aid in compensating the use of recycled source materials. It should be noted that the TE and RuL data are consistent with the bulk density data from Figure 2. Therefore, not only the redesign with regard to the added antioxidants, but also with regard to the overall packing density could have a positive effect on the performance at high temperatures.

Derived from Figure 6 and paralleling the R-curve data of the M-batches, the batches C-A and C-AR are promising for an in-depth evaluation in terms of the mechanical properties at elevated temperatures. For this reason, they are focused for the Young's modulus measurements as function of the temperature. The results are presented in Figure 7, both in absolute values and relative to the onset value after the coking process E_0. The room temperature trend of the Young's modulus is well reflected in the high-temperature data meaning the batch C-AR containing recycled material had a lower Young's modulus. This is fulfilled over the whole temperature range, regardless of whether during the heating, dwell or cooling segment.

To discuss the evolution of the Young's modulus, the following statements refer to the relative display in Figure 7b. While basically similar for temperatures below 1000°C, the Young's modulus curves of the batches C-A and C-AR differ above 1000°C and especially in the dwell segment.

A pronounced hysteresis behaviour was observed for both the C-A and C-AR material. The Young's modulus first decreases due to thermal expansion and a structural loosening of the entire structure (though without reducing the structural integrity as a whole), cf. region (i) of Figure 7b. However, it is less pronounced for C-AR than for C-A. Above 600°C, the Young's modulus increases in region (ii). Such a development was already observed for carbon-bonded ceramics before. Luchini et al. [38] traced it back to the closure of so-called "delamination gaps" between the ceramic particles (Al_2O_3 in their case) and the carbon matrix. This is accompanied by a densification of the structure. Such delamination gaps develop during the cooling step of the coking process due to the differences in the coefficient of thermal expansion of the ceramic particles and the carbon matrix. Theoretically, the closure should end at the coking temperature and then the Young's modulus

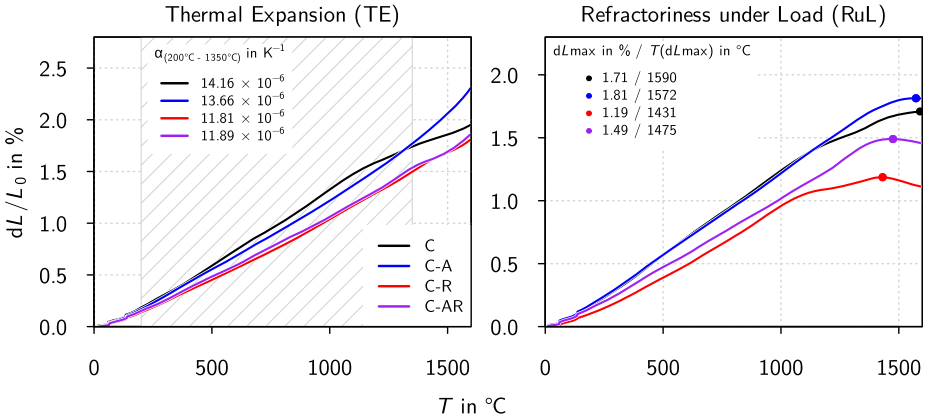

FIGURE 6 | Thermal expansion behaviour TE and refractoriness under load RuL of the coarse-grained MgO–C materials up to 1600°C (colour coding of the RuL identical to TE).

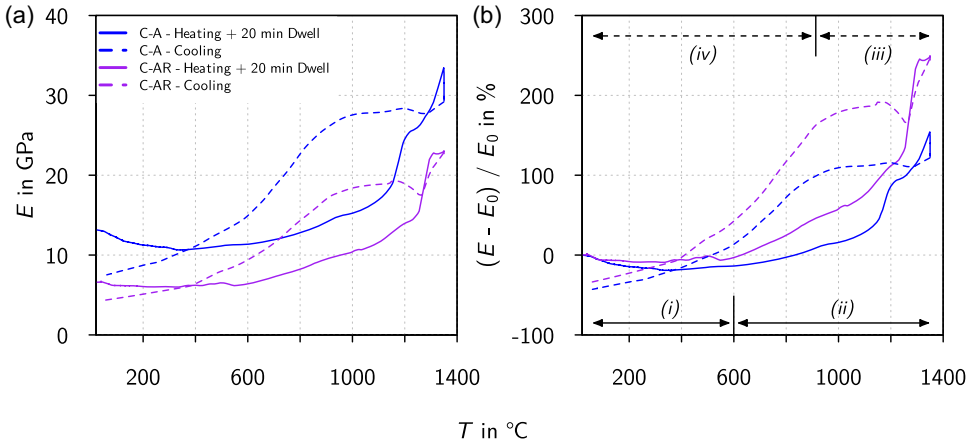

FIGURE 7 | Young's modulus of the coarse-grained MgO–C materials C-A and C-AR at elevated temperatures up to 1350°C under an argon atmosphere, (a) in absolute values and (b) relative to the onset value E_0 at room temperature.

should decrease again due to the overall structural loosening like in region (i). In the present case, the coking temperature was 1000°C, thus it becomes evident that the increase in the Young's modulus continues above 1000°C, thereby promoting further densification of the structure. This is further supported by the potential reactions of the antioxidants, for instance the reaction of Al_4C_3 from Al and the carbon as outlined in the introduction. Furthermore, the relative increase of the Young's modulus is higher for C-AR and a plateau is visible for temperatures above 1300°C for C-AR. Such plateau was not observed for C-A. Consequentially, the reactivity and thus the evolution of the Young's modulus is influenced by the source material. Another difference appears within the dwell segment. While the Young's modulus decreases for C-A over 20 min dwell time, the Young's modulus is about constant for C-AR during the dwell time. The latter would be in favour of a high-temperature application. In region (iii), a final difference was observed. C-A shows a plateau while C-AR had steep a drop followed by slight re-raising part of the $(E-E_0)/E_0$ curve. Below 950°C, both materials show a decrease in the Young's modulus, which fell below the initial value before the test, cf. region (iv). The latter was expected again due the mismatch of the thermal expansion of the ceramic particles and the carbon matrix, which again causes the delamination gaps mentioned before. Similar trends were observed by Luchini et al. [38] and also Luz et al. [24].

Clearly, the presented results were obtained under a protective argon atmosphere. In steel making, MgO–C refractories are frequently subjected to more oxidising atmospheres, at least insofar the refractory bricks ar not below the melt or slag level. When exposed to the oxidising atmospheres, volatilisation of the carbon and the formation of CO and/or CO_2 have to be taken into account. As a consequence, the structure of the MgO–C is altered, which clearly affects the material properties. Despite it is out of the scope of the present study to enter a comprehensive study of oxidation behaviour, the maximum carbon loss of the C-batches at 1600°C was studied. Coked spare samples of all C-batches were heated up to 1600°C, dwelled for 10 min. The carbon loss was derived from the mass difference before and after the thermal treatment and is present in Table 4.

As presented, the carbon loss is lower for the C-batches with antioxidants, which was expected according to the literature [10]. As a consequence of the oxidation, the binding matrix is removed whereby porosity is generated to the same extent. That would ultimately lower the high-temperature properties such as the RuL or the Young's modulus at elevated temperatures. To which extend and at which dwell times sintering effects may become relevant that could buffer this decrease in the high-temperature properties could be included in future studies on the subject.

TABLE 4 | Carbon loss after thermal treatment at 1600°C (derived from the relative mass change Δm).

	C	C-A	C-R	C-AR
Δm in ma%	6.7 ± 0.7	4.1 ± 2.2	8.3 ± 0.6	5.9 ± 0.4

3.4 | Overall Influence of the Carbon Content

A closing comment shall be made on the role of the overall carbon content. Intentionally, the amounts of the added graphite and carbon black were not adjusted to account for the carbon contained in the recycled FM source material. Hence, the carbon content of the batches M-R, M-AR, C-R and C-AR is higher. The extra carbon, contained in the R-FM source material fractions, amounted to 16.762 ma% for R-FM, 0–1 mm < 150 µm,[4] 13.811 ma% for R-FM, 0–1 mm, 10.241 ma% for R-FM, 1–3 mm and 16.812 ma% for R-FM, 3–6 mm. In correlation to the batch compositions from Table 1, the M-R and M-AR batches contained an extra of approximately 6.5 ma% of carbon when compared to M and M-A. For C-R and C-AR an extra of approximately 5.0 ma% of carbon was derived (in comparison to C and C-A). Nonetheless, the intention was to only modify the batches as less as possible to highlight the impact of the recycled source material, considering the extra carbon as an intrinsic feature of the recycled source material. Hence, for the final industrial application, a re-design of the batch composition should be undertaken to account for the carbon content of the recycled source material in order to equal the composition of common MgO–C bricks. By reducing the carbon content to the common amount, the number of carbon–ceramic interfaces would be lower and the mechanical interlocking of the ceramic particles would become more pronounced and favours the crack resistance. Besides, to enhance/toughen the carbon matrix network by an

additional agent could be a promising approach to further increase the brick durability. Such agents could be carboxylic acids, for example citric acid [19].

4 | Conclusion

In this study, MgO–C materials produced from recycled MgO–C source materials (up to 50%) and environmentally friendly binders additionally containing antioxidants were evaluated for their fracture behaviour and refractory properties in comparison with merely fresh MgO–C materials without antioxidants. As a novel feature, the fracture behaviour of the fine-grained matrix could be isolated. By computer-controlled sequential bending tests, conducted at deflection rates of only 0.02 µm s^{-1}, fracture resistances in KPa$\sqrt{m}$-range could be measured. The use of recycled source materials resulted in a less pronounced R-curves and lower K_{IR}. However, the addition of antioxidants can compensate this reduction. Apart from that, differences were observed in the refractoriness under load (RuL) and the thermal expansion (TE). Those are in good agreement with the R-curve results. From an engineering point of view and when combined with antioxidants, using recycled MgO–C as source material substitute is thus a promising concept for the recycled MgO–C to re-enter the refractory cycle. Nevertheless, further refinements regarding the batch composition are necessary, for example with regard to the total carbon content or by strengthening the carbon network in the matrix through additional additives.

Author Contributions

Marc Neumann: conceptualisation (lead), data curation (lead), formal analysis (lead), investigation (lead), methodology (lead), software (lead), validation (lead), visualisation (lead), writing – original draft (lead), writing – review & editing (equal). **Tom Weber**: data curation (supporting), formal analysis (supporting), investigation (supporting), writing – review & editing (supporting). **Jana Hubálková**: investigation (equal), methodology (equal), validation (equal), writing review & editing (supporting). **Florian Kerber**: data curation (equal), investigation (equal), writing – review & editing (supporting). **Dinesh Kumar Gunasekar**: formal analysis (equal), methodology (equal), writing – review & editing (equal). **Hans Jelitto**: data curation (equal), validation (equal), writing – review & editing (equal). **Christos G. Aneziris**: conceptualisation (lead), funding acquisition (lead), project administration (lead), resources (lead), supervision (lead), writing – review & editing (equal).

Acknowledgments

The authors thank Prof. Dr. G. A. Schneider, A. Borchert and M. Geerken for the support and opportunity to perform the sequential bending experiments at the Hamburg University of Technology. Beyond that, the authors want to credit Ms. M Arnold and Dr. C. Weigelt for their support in performing the DSC-TG and combustion analysis. This study was performed within the framework of the Research Training Group GRK 2802 "Refractory Recycling: A contribution for source material-, energy- and climate-efficiency in high temperature processes" (project number 461482547), funded by the German Research Foundation (DFG), PhD project P1 cohort II.

Open Access funding enabled and organized by Projekt DEAL.

Funding

This work was supported by Deutsche Forschungsgemeinschaft (461482547).

Conflicts of Interest

The authors declare no conflicts of interest.

Data Availability Statement

The data that support the findings of this study are available from the corresponding author upon reasonable request.

Endnotes

[1] The carbon content of the recycled R-FM 0–1 mm < 150 µm source material was determined by the aid of DSC-TG up to 1200°C (NETZSCH STA 409 PC/PG, Netzsch, Germany; heating rate: 10 K min^{-1}; synthetic air atmosphere). To verify the acquired DSC-TG data, the carbon content of the R-FM 0–1 mm < 150 µm source material was also evaluated by the aid of combustion analysis in a LECO CS244 (LECO Corporation, USA). The carbon content of the remaining R-FM source material fractions was derived from Lauermannova et al. [4].

[2] The Young's modulus, required during the data interpretation of the sequential bending tests, could not be determined for the individual samples in the coked state due to the notch. A subsequent work around based on the data of the sequential bending tests is presented in the appendix.

[3] Due to the overall low Young's modulus of the carbon-bonded magnesia materials, the course of the initial stage of the R-curve could stem from settling effects of the support rollers, i.e. an indentation of the lower hard metal supporting rollers into the ceramic material. Such an indentation would falsely add to the measured deflection. According to the Hertzian theory, the indentation depth depends on the applied load. To account for that indentation, the deflection data of all of the sequential bending experiments was corrected based on the applied load [40, 41]. Consequently, the presented data is already corrected for the settling indentation and the initial stage behaviour is nonetheless visible

[4] This could verified by combustion analysis of the R-FM, 0–1 mm < 150 µm resulting a carbon content of 16.192 ± 0.225 ma%. Hence the estimation via DSC-TG is considered as a reasonable method for determining the carbon content of the source materials.

References

1. M. Yellishetty, P. Ranjith, and A. Tharumarajah, "Iron ore and Steel Production Trends and Material Flows in the World: Is This Really Sustainable?," *Resources, Conservation and Recycling* 54 (2010): 1084–1094.

2. World Steel Association: World Steel in Figures 2025, *World Steel in Figures 2025* (World Steel Association, 2025), https://worldsteel.org/data/world-steel-in-figures/world-steel-in-figures-2025/.

3. L. Horckmans, P. Nielsen, P. Dierckx, and A. Ducastel, "Recycling of Refractory Bricks Used in Basic Steelmaking: A Review," *Resources. Conservation and Recycling* 140 (2019): 297–304.

4. A. Lauermannová, O. Jankovský, T. Stadtmüller, E. Storti, and C. Aneziris, "Eco-Friendly Lactose/Tannin-Based Binder in MgO–C Refractories Produced from MgO–C Recyclate," *Ceramics International* 50 (2024): 40823–40829.

5. K. Moritz, N. Brachhold, F. Küster, S. Dudczig, T. Schemmel, and C. Aneziris, "Studies on the use of Two Different Magnesia-Carbon Recyclates as Secondary Raw Material for MgO–C Refractories," *Open Ceramics* 15 (2023): 100426.

6. N. C. Saha, F. Bhunia, and A. Kaviraj, "Toxicity of Phenol to Fish and Aquatic Ecosystems," *Bulletin of Enviromental Contamination and Toxicology* 63 (1999): 195–202.

7. T. Stadtmüller, E. Storti, N. Brachhold, et al., "MgO–C Refractories Based on Refractory Recyclates and Environmentally Friendly Binders," *Journal of the European Ceramic Society* 16 (2023): 100469.

8. J. Rodgriguez-Marisol, T. Cordero, and J. J. Rodriguez, "High-Temperature Carbons From Kraft Lignin," *Carbon* 34, no. 1 (1996): 43–52.

9. S. Zhang, N. Marriott, and W. Lee, "Thermochemistry and Microstructures of MgO–C Refractories Containing Various Antioxidants," *Journal of the European Ceramic Society* 21 (2001): 1037–1047.

10. C. Aneziris, J. Hubálková, and R. Barabás, "Microstructure Evaluation of MgO–C Refractories with TiO_2- and Al-Additions," *Journal of the European Ceramic Society* 27 (2007): 73–78.

11. A. Gokce, C. Gurcan, S. Ozgen, and S. Aydin, "The Effect of Antioxidants on the Oxidation Behaviour of Magnesia-Carbon Refractory Bricks," *Ceramics International* 34 (2008): 323–330.

12. L. Musante, L. Martorello, P. Galliano, A. Cavalieri, and A. Tomba Martinez, "Mechanical Behaviour of MgO–C Refractory Bricks Evaluated by Stress-Strain Curves," *Ceramics International* 38 (2012): 4035–4047.

13. Y. Hino and S. Zhang, "Effects of Carbon Content and Grain Orientation on the Crack Growth Behaviour in Magnesia-Carbon Refractory Bricks," *ISIJ International* 54, no. 10 (2014): 2221–2229.

14. G. Wei, B. Zhu, X. Li, and Z. Ma, "Microstructure and Mechanical Properties of Low-Carbon MgO–C Refractories Bonded by an Fe Nanosheet-Modified Phenol Resin," *Ceramics International* 41 (2015): 1553–1566.

15. C. S. Bitencourt, A. P. Luz, C. Pagliosa, and V. C. Pandolfelli, "Phase and Microstructural Evolution Based on Al, Si and TiO_2 Reactions with a MgO–C Resin-Bonded Refractory," *Ceramics International* 42 (2016): 10480–16490.

16. T. Zhu, L. Yawei, and S. Sang, "Heightening Mechanical Properties and Thermal Shock Resistance of Lowecarbon Magnesiaegraphite Refractories through the Catalytic Formation of Nanocarbons and Ceramic Bonding Phases," *Journal of Alloys and Compounds* 783 (2019): 2500–2509.

17. M. Ludwig, E. Sniezek, I. Jastrzebska, et al., "Recycled Magnesia-Carbon Aggregate as the Component of New Type of MgO–C Refractories," *Construction and Building Materials* 272 (2021): 121912.

18. A. Schramm, L. Knöchel, T. Schemmel, C. Aneziris, A. Weidner, and H. Biermann, "Four-Point Bending Tests at High Temperatures on Commercial MgO–C Refractory Bricks with and Without Recyclate Considering Different Carbon Contents," *Advanced Engineering Materials* 54, no. 1–12 (2025): e202502715.

19. C. G. Aneziris, D. K. Gunarsekar, P. Gehre, D. Veres, S. Dudczig, and J. Hubálková, *German Patent Application no. 10 2025 120 670.8* (2025).

20. M. Lugovy, N. Orlovskaya, M. Neumann, et al., "Room Temperature R-Curve and Stable Crack Growth Behaviour of ZrB_2-SiC Ceramic Composites," *Advances in Applied Ceramics* 118, no. 4 (2019): 169–182.

21. M. Neumann, P. Gehre, J. Kuebler, et al., "Stable Crack Propagation in Free Standing Thermal Sprayed Al_2O_3 and Al_2O_3-ZrO_2-TiO_2 Coatings," *Ceramics International* 45, no. 7 (2019): 8761–8766.

22. M. Neumann, J. Hubálková, F. Kerber, P. Gehre, H. Jelitto, and C. Aneziris, "Impact of Thermal Shock on the R-Curve and Subcritical Damage Behaviour of Flame-Sprayed Alumina Compounds," *Journal of the European Ceramic Society* 44 (2024): 3418–3428.

23. R Core Team, *R: A Language and Environment for Statistical Computing* (R Foundation for Statistical Computing, 2024).

24. A. Luz, T. Souza, C. Pagliosa, M. Brito, and V. Pandolfelli, "In Situ Hot Elastic Modulus Evolution of MgO–C Refractories Containing Al, Si or Al–Mg Antioxidants," *Ceramics International* 42 (2016): 9836–9843.

25. M. Khezrabadi, J. Javadpour, H. Rezaie, and R. Naghizadeh, "The Effect of Additives on the Properties and Microstructures of Al_2O_3–C Refractories," *Journal of Materials Science* 41 (2006): 3027–3032.

26. S. Fünfschilling, T. Fett, M. J. Hoffmann, et al., "Mechanisms of Toughening in Silicon Nitrides: The Roles of Crack Bridging and Microstructure," *Acta Materialia* 59 (2011): 3978–3989.

27. R. W. Steinbrech, A. Reichl, and W. Schaarwächter, "R-Curve Behavior of Long Cracks in Alumina," *Journal of the American Ceramic Society* 73, no. 7 (1990): 2009–2015.

28. T. Ogawa and J. LLorca, "Stable Crack Growth in Polycrystalline Magnesia under Monotonic and Cyclic Loads," *Journal of the American Ceramic Society* 77, no. 4 (1994): 961–969.

29. C. J. Gilbert, R. N. Petrany, R. O. Ritchie, and R. W. Steinbrech, "Cyclic Fatigue in Monolithic Alumina: Mechanisms for Crack Advance Promoted by Frictional Wear of Grain Bridges," *Journal of Materials Processing Technology* 30 (1995): 643–654.

30. S. Hayashi, H. Takahaschi, A. Watanabe, A. Osaka, and Y. Miura, "Dependence of Mechanical Properties of MgO–C Bricks on Graphite Content," *Journal of the Ceramic Society of Japan* 102, no. 1 (1994): 23–28.

31. Y. Hino, K. Yoshida, Y. Kiyota, and M. Kuwayama, "Fracture Mechanics Investigation of MgO–C Bricks for Steelmaking by Bending and Fatigue Failure Tests Along with X-Ray CT Scan Observation," *ISIJ International* 53, no. 8 (2013): 1392–1400.

32. H. Zielke, M. Abendroth, M. Kuna, and B. Kiefer, "Determining the Fracture Toughness of Ceramic Filter Materials Using the Miniaturized Chevron-Notched Beam Method at High Temperature," *Ceramics International* 44, no. 12 (2018): 13986–13993.

33. J. Solarek, A. Schramm, S. Henkel, A. Weidner, C. Aneziris, and H. Biermann, "Fracture Mechanics Behavior of Coarse-Grained MgO–C at Room and High Temperature," *Ceramics International* 49 (2023): 33874–33880.

34. H. Jelitto and G. A. Schneider, "A Geometric Model for the Fracture Toughness of Porous Materials," *Acta Materialia* 151 (2018): 443–453.

35. H. Jelitto and G. A. Schneider, "Extended Cubic Fracture Model for Porous Materials and the Dependence of the Fracture Toughness on the Pore Size," *Materialia* 12 (2020): 100761.

36. D. Munz and T. Fett, *Ceramics Mechanical Properties, Failure Behaviour, Materials Selection*. Springer Series in Material Science, vol. 36 (Springer-Verlag, 2001), 25–26.

37. H. El Attaoui, M. Saadaoui, J. Chevalier, and G. Fantozzi, "Quantitative Analysis of Crack Shielding Degradation During Cyclic Fatigue of Alumina," *Journal of the American Ceramic Society* 178, no. 1 (2005): 172–178.

38. B. Luchini, J. Grabenhorst, J. Fruhstorfer, V. C. Pandolfelli, and C. G. Aneziris, "On the Nonlinear Behavior of Young's Modulus of Carbon-Bonded Alumina at High Temperatures," *Journal of the American Ceramic Society* 101, no. 9 (2018): 4171–4183.

39. T. Fett and E. Diegele, "Indirect Measurements of Compliance in Four-Point-Bending Tests," *Journal of Testing and Evaluation* 16 (1988): 487–488.

40. M. Puttock and E. Thwaite, *Elastic Compression of Spheres and Cylinders at Point and Line Contact* (Commonwealth Scientific and Industrial Research Organization, 1969).

41. C. J. Collins, B. Yang, T. D. Crenshaw, and H.-L. Ploeg, "Evaluation of Experimental, Analytical, and Computational Methods to Determine Long-Bone Bending Stiffness," *Journal of the Mechanical Behavior of Biomedical Materials* 115 (2021): 104253.

Appendix

R-Curve Determination: Correction of the Young's Modulus

As briefly mentioned in the Experimental Section, the R-curve evaluation called for the Young's modulus of the beam sample tested. More precisely, the Young's modulus enters Equations (A1) – (A3) in the form of $E' = E(1-\nu)^{-1}$, which is employed to determine the crack length $a = a_r w$ [20, 36, 39]. In Equation (A1), the upper integration limit a_r is

evaluated iteratively for the release compliances $C(a_{r,re})$ which are determined from the release slopes $\zeta = C(a_{r,re})^{-1}$. The release slopes ζ are derived from the load-deflection-data of the sequential bending experiments (cf [21, 22].).

$$C(a_r) = \frac{9(s_2 - s_1)^2}{2E'bw^2} \int_0^{a_r} \frac{a'(\Gamma_M(a'))^2}{(1-a')^3} da' + C_0^* \tag{A1}$$

$$C_0^* = \left(\frac{s_2 - s_1}{w}\right)^2 \frac{1}{E'b} \left(\frac{s_2 + 2s_1}{4w} + \frac{(1+\nu)w}{2(s_2 + s_1)}\right) \tag{A2}$$

$$\Gamma_M(a_r) = \Gamma(1-a_r)^{1.5} = 1.1215\sqrt{\pi}\left[\frac{5}{8} - \frac{5}{12}a_r + \frac{1}{8}a_r^2 + 5a_r^2(1-a_r)^6 + \frac{3}{8}\exp\left(-6.1342\frac{a_r}{(1-a_r)}\right)\right] \tag{A3}$$

The Young's modulus was estimated as the median Young's modulus of the seventeen un-notched and coked beams, presented in Figure 2. Since the notch was incorporated into the sequential bending test samples prior to the coking step, these samples could not be tested using impulse excitation technology in their coked state. The notch conflicts with the requirements of the applicable standard DIN EN 843-2:2007 with regard to sample geometry. Like discussed by Neumann et al. [21], the resulting R-curve is sensitive to the Young's modulus, highlighting the importance of accurately determining the Young's modulus, if practicable.

To find an adequate Young's modulus, the following routine was implemented: When introducing a Young's modulus value that is lower than the 'correct' Young's modulus, a number of points of the R-curve data is clustering at crack extensions of 0 µm. However, the load-deflection curves of the initial loading sequences imply crack growth since they are already subdivided into a linear and a non-linear segment. Whenever the load-deflection curve of a loading sequence deviates from a linear course, crack growth is indicated. Hence, the Young's modulus has to be increased iteratively until the before mentioned clustering is no longer evident in the resulting R-curve data (for the first time). By this iterative process, the Young's modulus is varied until crack extension starts at the notch depth. This complies with the reconstructed CT images, where the crack was traced originating from the notch ground. When the Young's modulus is increased beyond that point, the R-curve is shifted towards higher values of crack extension and crack resistance. This should be avoided since it poses an over-estimation of the R-curve, which could be fatal. The effect of different Young's moduli on the resulting R-curve data is presented in Figure A1 (exemplarily for the *B*-type measurement of M-AR). The starting value of the Young's modulus was set to 1.00 GPa as a sufficiently low starting value and the increment size was set to 0.05 GPa.

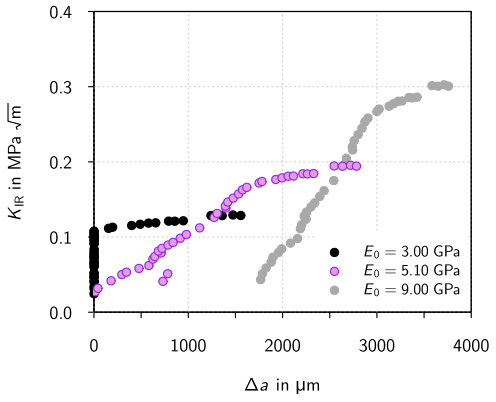

FIGURE A1 | Influence of Young's modulus E_0 on the resulting R-curve, exemplarily shown for the *B*-type measurement of the M-AR batch (E_0 = 3.00 GPa-Young's modulus too low, clustering observed; E_0 = 5.10 GPa-Young's modulus adequate, no clustering observed; E_0 = 9.00 GPa-Young's modulus too high, overestimation).